Equilibrium, Stability, and Dynamics of Rectangular Liquid-Filled Vessels

Russell Trahan III
e-mail: rtrahan3@tamu.edu

Tamás Kalmár-Nagy
e-mail: jcnd@kalmarnagy.com

Department of Aerospace Engineering,
Texas A&M University,
College Station, TX 77843

Here we focus on the stability and dynamic characteristics of a rectangular, liquid-filled vessel. The position vector of the center of gravity of the liquid volume is derived and used to express the equilibrium angles of the vessel. Analysis of the potential function determines the stability of these equilibria, and bifurcation diagrams are constructed to demonstrate the co-existence of several equilibrium configurations of the vessel. To validate the results, a vessel of rectangular cross section was built. The results of the experiments agree well with the theoretical predictions of stability. The dynamics of the unforced and forced systems with a threshold constraint is discussed in the context of the nonlinear Mathieu equation. [DOI: 10.1115/1.4003915]

1 Introduction

Determining equilibrium positions of structures and characterizing their stability is a common engineering task. Fluid-structure interactions are one of the many stability concerns in dynamic systems. For example, some marine structures such as floating oil rigs and dry-docks use water as ballast to stabilize the structure. Vehicles such as aircraft, boats, and machinery operate under conditions where the fuel tank or liquid payload may adversely affect the stability of the vehicle due to sloshing [1]. Determining the behavior of the liquid in a tank is an important consideration in the design and analysis of these devices. These examples provide the motivation for our stability analysis and dynamic modeling of a rectangular liquid-filled vessel.

This paper discusses the static stability and simplified equation of motion of a vessel with a rectangular cross section that can pivot about a fixed point and contains liquid. The emphasis with the equation of motion is the state constraint representative of the liquid spilling from the vessel. An equally important purpose for this paper is to present an example through which the concepts of bifurcations, potential functions, and stability of nonlinear physical systems become more available to students. The experimental setup described here is easy to build and may serve as an effective classroom demonstration. A similar system—a hanging block—is studied by Stépán and Bianchi [2]. They characterized the stability of a mass hanging from two ropes by using a potential function depending on various geometric parameters of the system.

Research into the stability of floating bodies has a long history, starting with Archimedes' *On Floating Bodies.* The ship problem relates the buoyancy force to ship stability. Locating equilibrium positions of floating objects and ascertaining the stability of these equilibria is not a trivial exercise. Duffy [3] considered the equilibrium positions of partially submerged rods supported at one end and showed the existence of simple bifurcations and the jump phenomenon (hysteresis) in the problem. Erdös et al. [4] investigated the equilibrium configurations for floating solid prisms of square and equilateral triangular cross section. Delbourgo [5] provided a solution to the metacentric problem for a floating plank. Our system can be thought of as an inverted ship problem (for the ship problem, the body is submerged in the liquid). While Delbourgo's problem is analogous to ours and his results are similar, we believe that our exposition is more detailed and lucid, thereby making this type of problem more known to the nonlinear dynamics community.

Manuscript received May 28, 2010; final manuscript received March 31, 2011; published online May 20, 2011. Assoc. Editor: Bala Balachandran.

We start by defining the geometry of the vessel and the liquid contained within in Sec. 2. The physical parameters that are varied are the amount of liquid, the pivot height to vessel-width ratio, and the angle of rotation about the pivot. The algebraic equations describing the location of the center of gravity of the liquid are derived. From these equations, the equilibrium positions of the vessel are expressed in Sec. 3. The stability of the equilibrium positions is determined with a potential function in Sec. 3.2. The results from the equilibrium calculations and stability analysis are used to construct bifurcation diagrams for various physical parameters of the vessel in Sec. 4. These diagrams are then compared with experimental data in Sec. 5. Lastly a simplified equation of motion is presented in Sec. 6. The response of the system and the state constraint are discussed in Sec.7.

2 Problem Definition and Assumptions

The object of our study (hereupon called vessel) is illustrated in Fig. 1. We first determine the static equilibrium states of the vessel-liquid system and their stability. We then turn our focus to the rotational dynamics of the vessel. Fluid dynamic effects are excluded, specifically sloshing of the liquid. We assume that the walls of the vessel have negligible thickness and mass. Furthermore, we define the *spill threshold* as the rotational state where the liquid would begin to spill out of the top of the vessel.

The vessel has a rectangular cross section—characterized by the width W—and contains a liquid with cross-sectional area of $H \cdot W$. The distance of the pivot from the base is P. Figure 2 depicts a situation when the vessel is rotated about the pivot by angle θ. Hereon, we illustrate the liquid rotated and the vessel stationary for simplicity.

All parameters are nondimensionalized by scaling with the pivot height P, i.e.,

$$h = \frac{H}{P} \tag{1}$$

$$w = \frac{W}{P} \tag{2}$$

Without loss of generality (due to the symmetry of the vessel), we will assume non-negative θ in the calculations. Using the coordinate system defined in Fig. 2, the position vectors for the bottom corners of the vessel, A and B, relative to O can be expressed in terms of $\theta \geq 0$ as

$$\vec{r}_A = \left(\sin\theta - \frac{w}{2}\cos\theta\right)\hat{i} - \left(\cos\theta + \frac{w}{2}\sin\theta\right)\hat{j} \tag{3}$$

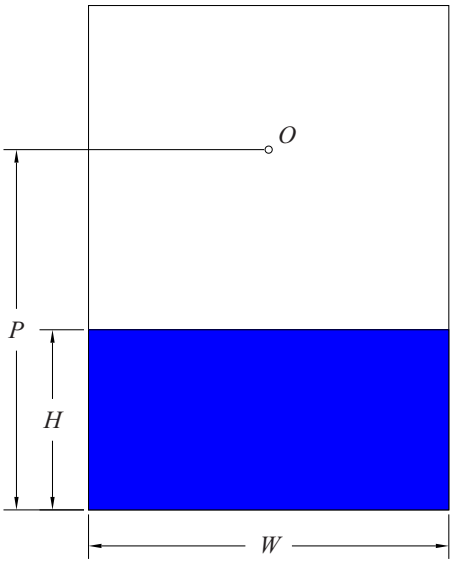

Fig. 1 Vessel geometry

$$\vec{r}_B = \left(\sin\theta + \frac{w}{2}\cos\theta\right)\hat{i} - \left(\cos\theta + \frac{w}{2}\sin\theta\right)\hat{j} \tag{4}$$

These expressions will later be used to derive the location of the center of gravity (CG) of the liquid cross section.

2.1 Geometric Cases. The shape of the liquid's cross-section is dependent on the pivot angle θ and amount of liquid in the vessel. The cross section could either be trapezoidal (Fig. 3(*a*)) or triangular (Fig. 3(*b*)), referred to as case 1 and case 2, respectively.

The triangular section of liquid is defined by the points A, E, and F. The relative positions of points E and F with respect to A are expressed by

$$\boldsymbol{r}_{E/A} = \max\left(w, \sqrt{2\frac{hw}{\tan\theta}}\right)\hat{i}' \tag{5}$$

$$\boldsymbol{r}_{F/A} = \sqrt{2hw\tan\theta}\,\hat{j}' \tag{6}$$

Equation (5) expresses that $r_{E/A} = |\boldsymbol{r}_{E/A}|$ is physically limited to the vessel-width, i.e., $r_{E/A} \leq w$. This constraint results in the two cases

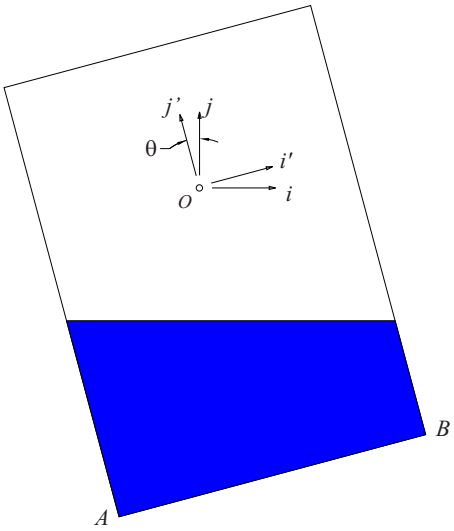

Fig. 2 Liquid cross section geometry

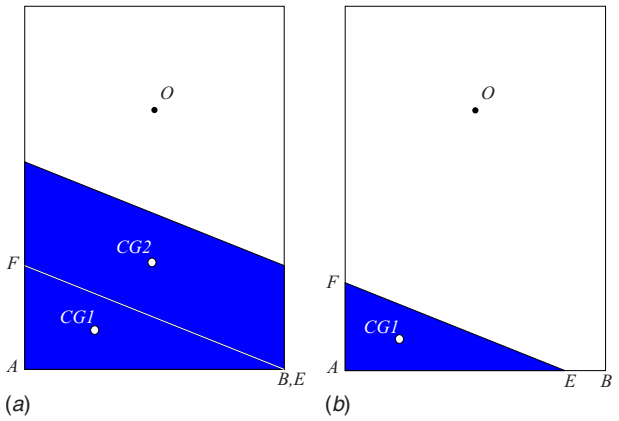

Fig. 3 Vessel cases

mentioned above, i.e., trapezoidal (case 1) or triangular (case 2) cross section, characterized by the inequalities

$$\text{case 1:} \quad \tan\theta < \frac{2h}{w} \tag{7}$$

$$\text{case 2:} \quad \tan\theta \geq \frac{2h}{w} \tag{8}$$

2.2 Center of Gravity. The equilibria of the vessel are determined by first finding the CG of the liquid. CG1 (see Fig. 3) is located at the centroid of the triangle, and CG2 is located at the centroid of the parallelogram.

$$\boldsymbol{r}_{\mathrm{CG1}} = \left[\left(\frac{\sqrt{2}}{3}\sqrt{\frac{hw}{\tan\theta}} - \frac{w}{2}\right)\cos\theta + \left(1 - \frac{\sqrt{2hw\tan\theta}}{3}\right)\sin\theta\right]\hat{i} + \left[\left(\frac{\sqrt{2hw\tan\theta}}{3} - 1\right)\cos\theta + \left(\frac{\sqrt{2}}{3}\sqrt{\frac{hw}{\tan\theta}} - \frac{w}{2}\right)\sin\theta\right]\hat{j} \tag{9}$$

$$\boldsymbol{r}_{\mathrm{CG2}} = \left(1 - \frac{w\tan\theta}{4} - \frac{h}{2}\right)\sin\theta\hat{i} + \left(\left(\frac{h}{2} - 1\right)\cos\theta + \frac{w}{4}\sin\theta\right)\hat{j} \tag{10}$$

The CG for the whole liquid cross section is calculated using a weighted average of the coordinates of the two CGs and the corresponding areas A_1 and A_2, i.e.,

$$\boldsymbol{r}_{\mathrm{CG}} = \frac{\boldsymbol{r}_{\mathrm{CG1}}A_1 + \boldsymbol{r}_{\mathrm{CG2}}A_2}{A_1 + A_2} \tag{11}$$

where the areas are

$$A_1 = \begin{cases} \frac{1}{2}w^2\tan\theta & \text{case 1} \\ hw & \text{case 2} \end{cases}$$

$$A_2 = \begin{cases} hw - \frac{1}{2}w^2\tan\theta & \text{case 1} \\ 0 & \text{case 2} \end{cases} \tag{12}$$

The center of gravity of the liquid cross section is thus given by

$$\boldsymbol{r}_{CG}=\begin{cases}\left(1-\dfrac{w^2\tan^2\theta}{24h}-\dfrac{w^2}{12h}-\dfrac{h}{2}\right)\sin\theta\,\hat{i}+\left(\left(\dfrac{h}{2}-1\right)\cos\theta+\dfrac{w^2\tan\theta\sin\theta}{24h}\right)\hat{j} & \text{case 1}\\ \left[\left(\dfrac{\sqrt{2}}{3}\sqrt{\dfrac{hw}{\tan\theta}}-\dfrac{w}{2}\right)\cos\theta+\left(1-\dfrac{\sqrt{2hw\tan\theta}}{3}\right)\sin\theta\right]\hat{i}+\left[\left(\dfrac{\sqrt{2hw\tan\theta}}{3}-1\right)\cos\theta+\left(\dfrac{\sqrt{2}}{3}\sqrt{\dfrac{hw}{\tan\theta}}-\dfrac{w}{2}\right)\sin\theta\right]\hat{j} & \text{case 2}\end{cases} \tag{13}$$

3 Potential Function, Equilibria, and Stability

The equilibrium angles of the vessel and their stability are determined by analyzing the nondimensional potential function [6] defined by the $\hat{j}$ component of the CG location:

$$U\equiv\boldsymbol{r}_{CG}\cdot\hat{j}=\begin{cases}\left(\dfrac{h}{2}-1\right)\cos\theta-\dfrac{w^2\tan\theta\sin\theta}{24h} & \text{case 1}\\ \left(\dfrac{\sqrt{2hw\tan\theta}}{3}-1\right)\cos\theta+\left(\dfrac{\sqrt{2}}{3}\sqrt{\dfrac{hw}{\tan\theta}}-\dfrac{w}{2}\right)\sin\theta & \text{case 2}\end{cases} \tag{14}$$

Physically, the vessel is in equilibrium when the CG of the cross section of the liquid is on the vertical axis. This is expressed as $\boldsymbol{r}_{CG}\cdot\hat{i}=0$ It is also true that $\boldsymbol{r}_{CG}\cdot\hat{i}=0$ corresponds to local extrema of the potential function, i.e.,

$$\frac{dU}{d\theta}=0=\begin{cases}\left(1-\dfrac{w^2\tan^2\theta}{24h}-\dfrac{w^2}{12h}-\dfrac{h}{2}\right)\sin\theta & \text{case 1}\\ \dfrac{\sqrt{2hw}}{3}-\dfrac{w}{2}\tan^{1/2}\theta+\tan^{3/2}\theta-\dfrac{\sqrt{2hw}}{3}\tan^2\theta & \text{case 2}\end{cases} \tag{15}$$

In Sec. 3.2, we will use the second derivative of the potential function to classify the stability of particular equilibria.

3.1 Equilibria Conditions. Plotted in Fig. 4 are the nonzero equilibrium positions given by Eq. (15) in $h-w-\theta$ space. The left and right shaded regions depict case 2 and case 1 equilibria, respectively.

As can be observed, for given values of h and w, multiple θ solutions can exist. We now define the domains in which different numbers of equilibria exist.

Case 1 equilibria are determined by (see Eq. (15))

$$\left(1-\frac{w^2\tan^2\theta}{24h}-\frac{w^2}{12h}-\frac{h}{2}\right)\sin\theta=0,\quad 0\le\tan\theta<\frac{2h}{w} \tag{16}$$

Clearly, $\theta=0$ is always a solution. Other solutions satisfy

$$\tan^2\theta=(2h-h^2)\frac{12}{w^2}-2,\quad 0<\tan\theta<\frac{2h}{w} \tag{17}$$

Expression (17) is equivalent to the two inequalities:

$$(h-1)^2+\frac{w^2}{6}\le 1 \tag{18}$$

$$\left(h-\frac{3}{4}\right)^2+\frac{w^2}{8}\ge\frac{9}{16} \tag{19}$$

which determine that a positive θ solution exists between the two half-ellipses shown in Fig. 5. For later reference, we refer to equation $[h-(3/4)]^2+(w^2/8)=(9/16)$ as curve I.

Case 2 equilibria are given by

$$\frac{\sqrt{2hw}}{3}-\frac{w}{2}\tan^{1/2}\theta+\tan^{3/2}\theta-\frac{\sqrt{2hw}}{3}\tan^2\theta=0 \tag{20}$$

subject to the constraint

$$\tan\theta\ge\frac{2h}{w} \tag{21}$$

It can be shown that Eq. (20) has three non-negative roots. The regions in h-w space with one or three *real* roots are separated by a curve on which Eq. (20) has a double root. For Eq. (20) to have a double root it is necessary that its derivative vanishes, i.e.,

$$-3w+18\tan\theta-8\sqrt{2}\sqrt{hw}\tan^{3/2}\theta=0. \tag{22}$$

Equations (20) and (22) are now combined and solved for h and w to give the boundary in parametric form in terms of θ as

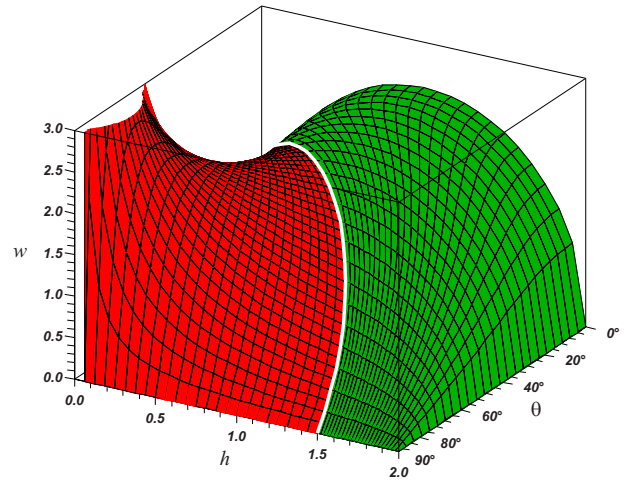

Fig. 4 $h-w-\theta$ plot of $\theta\neq 0$ equilibria

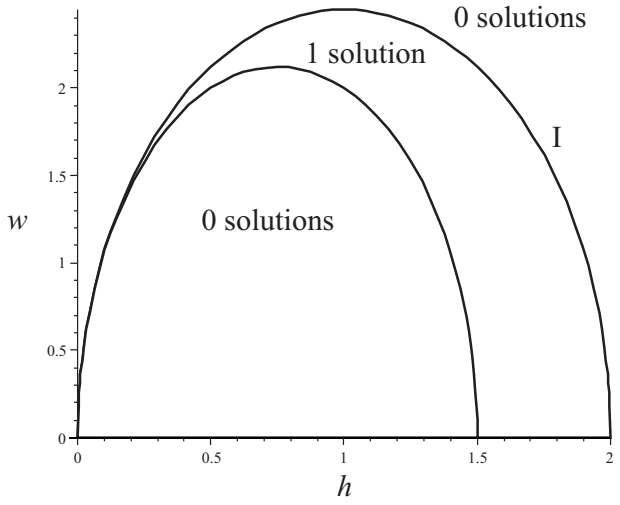

Fig. 5 Number of solutions of expression (17)

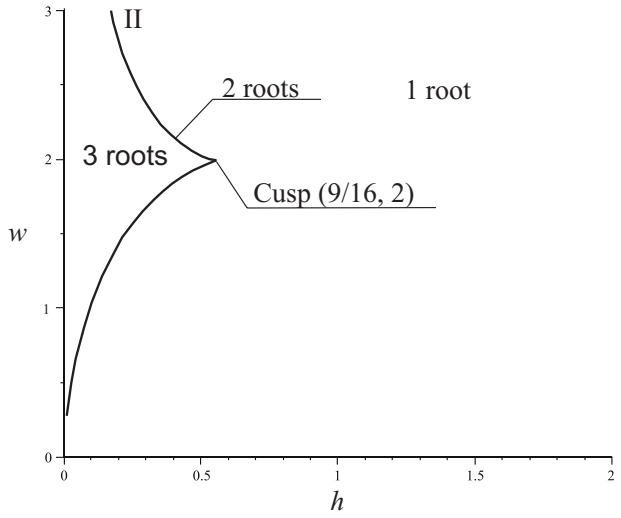

Fig. 6 Number of real roots in Eq. (20)

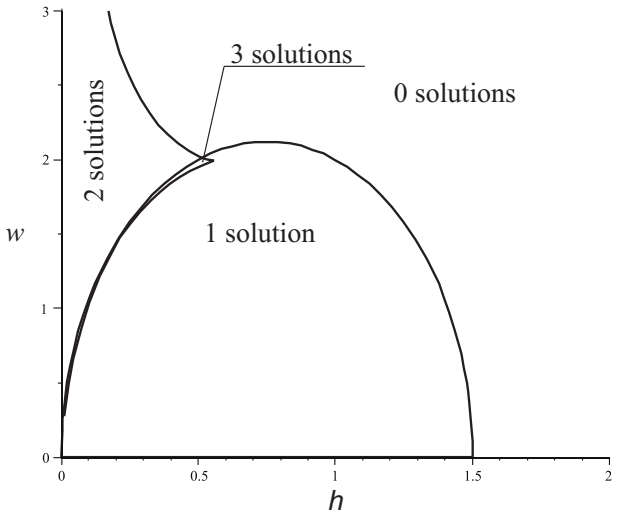

Fig. 7 Number of solutions in Eq. (20) with constraint (21)

$$h(\theta) = \frac{9\tan^2\theta}{(\tan^2\theta + 3)(3\tan^2\theta + 1)} \tag{23}$$

$$w(\theta) = \frac{2\tan\theta(\tan^2\theta + 3)}{3\tan^2\theta + 1} \tag{24}$$

The parametric curve $\{h(\theta), w(\theta)\}$, referred to as curve II, is plotted in Fig. 6. The region left of the curve is where Eq. (20) has three real roots.[1]

Substituting the constraint (21) into Eq. (20) gives

$$-12h^{3/2}\sqrt{w} + 8h^{5/2}\sqrt{w} + \sqrt{h}w^{5/2} \geq 0 \tag{25}$$

which can also be expressed as

$$\left(h - \frac{3}{4}\right)^2 + \frac{w^2}{8} \leq \frac{9}{16} \tag{26}$$

Outside of this elliptical region (bounded by curve I), one of the possible real roots does not satisfy constraint (21). Figure 7 shows the number of valid case 2 solutions in the h-w plane.

We are now in a position to present information about all equilibria of the vessel. Recall that in the calculations θ was assumed to be non-negative. Without this restriction each case 1 and case 2 solution corresponds to two equilibrium configurations of the vessel, resulting in an odd number of equilibria for the system ($\theta = 0$, case 1, and case 2 equilibria). Figure 8 shows the various regions and indicates the total number of equilibria. The gray region is where case 2 equilibria are present.

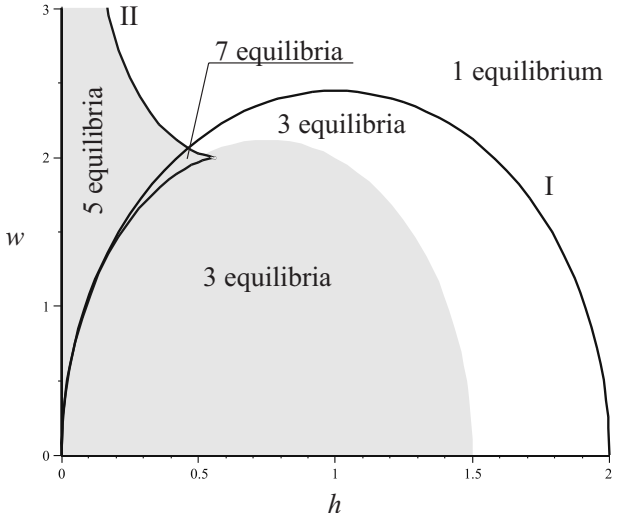

Fig. 8 Total number of equilibria for the vessel in terms of *h* and *w*. Solid lines demarcate regions with different numbers of equilibria. The shaded region refers to the validity domain of case 2.

3.2 Stability Conditions. An equilibrium position is stable or unstable if the second derivative of the potential function evaluated at the equilibrium is positive or negative, respectively (corresponding to a local minimum or maximum of the potential function) [6]. The second derivative of the potential function (14) is

$$\frac{d^2U}{d\theta^2} = \begin{cases} \left(1 - \frac{h}{2}\right)\cos\theta - \frac{w^2}{24h}(2\cos\theta + 3\sin^2\theta\cos^{-1}\theta + 2\sin^4\theta\cos^{-3}\theta) & \text{case 1} \\ -\frac{\sqrt{2hw}}{6}(\sin^{5/2}\theta\cos^{-3/2}\theta + 6\sin^{1/2}\theta\cos^{1/2}\theta + \sin^{-3/2}\theta\cos^{5/2}\theta) + \cos\theta + \frac{w}{2}\sin\theta & \text{case 2} \end{cases} \tag{27}$$

[1]This statement can be proved by considering the $h=0$, $w=2$ case. Equation (20) reduces to $\tan^3\theta - \tan\theta = 0$, which clearly has three real roots. By a continuity argument, Eq. (20) has three real roots in the region left of the double root curve.

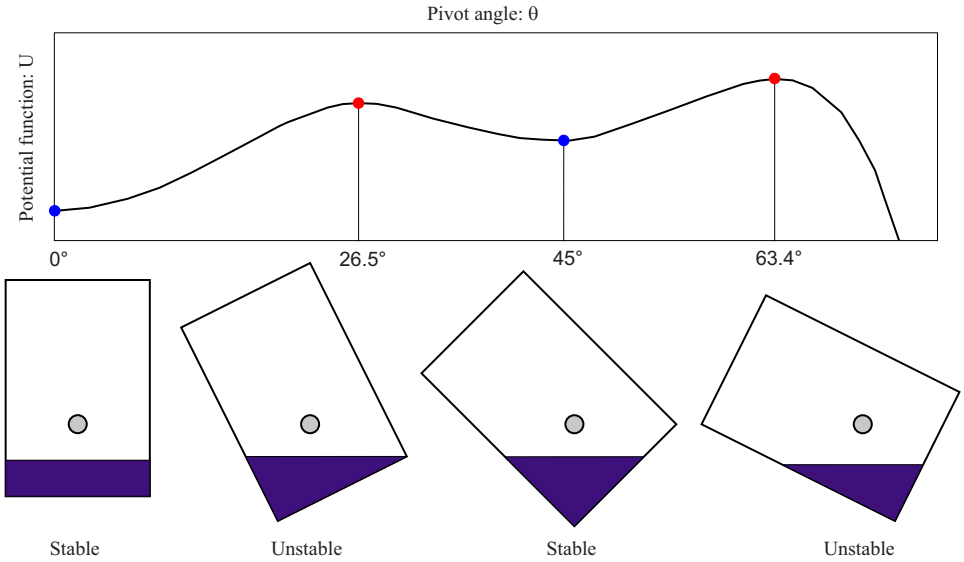

Fig. 9 Coexistence of equilibria for $w=2$, $h=0.5$

The stability condition for $\theta=0$ assumes a particularly simple form

$$\left.\frac{d^2U}{d\theta^2}\right|_{\theta=0} = 1 - \frac{h}{2} - \frac{w^2}{12h} > 0 \tag{28}$$

$$(h-1)^2 + \frac{w^2}{6} < 1 \tag{29}$$

The $\theta=0$ equilibrium is therefore stable inside the elliptical region bounded by curve I in Fig. 8. Even though the stability criterion (29) is local in nature, it also provides *global* information about the stability of all system equilibria. Maxima and minima of a one-dimensional potential function must alternate; however, it is possible for an inflection point to exist in between. This implies that the stability of all equilibria can be determined based on the stability of the $\theta=0$ case alone.

To further illustrate the coexistence of equilibria for a pair of h and w and their alternating stability, Fig. 9 depicts the $\theta \geq 0$ equilibria for $w=2$, $h=0.5$ and the corresponding potential function [7].

4 Bifurcations and Bifurcation Diagrams

A bifurcation, in general, refers to a qualitative change in system behavior [8]. In our context, this change is characterized by creation or destruction of equilibria. Based on the statements in Sec. 3.2, a change in the number of equilibria also corresponds to a change in the stability of a branch of equilibria. The point where the bifurcation occurs is referred to as the bifurcation point, which varies based on the parameters of the system.

To combine the information about the location and stability of equilibria, bifurcation diagrams are constructed. The bifurcation diagrams for several sets of parameters are shown in Fig. 10. Note that the full diagrams are symmetric about $\theta=0$.

There are several features on the bifurcation diagrams worth pointing out.

A *pitchfork bifurcation* [9] is formed when two equilibrium branches emanate from the $\theta=0$ equilibrium. In the previous section, we established that the $\theta=0$ equilibrium changes from stable to unstable by crossing curve I in the h-w parameter plane (Fig. 8), while two additional equilibria appear simultaneously. This pitchfork bifurcation is therefore subcritical. Similarly, we have a subcritical pitchfork by crossing the cusp at $w=2$, $h=9/6$ (Fig. 10(*c*)).

A *saddle-node (SN) bifurcation* is where stable and unstable equilibrium points annihilate one another [8]. This type of bifurcation appears in Fig. 10(*a*), 10(*b*), 10(*d*), and 10(*e*). The saddle-node bifurcations correspond to curve II (on which double roots of Eq. (20) exist) in Fig. 8. The co-existence of multiple stable branches in Figs. 10(*a*)–10(*d*) also implies that the stable position of the vessel can become path dependent while changing the liquid level. This is the so-called *hysteresis* phenomenon.

Figure 11 shows the region around the cusp in detail. The points *A*-*J* on the h-w plane are noted on bifurcation diagrams to explicitly show their respective number of equilibria. We also label the curves where SNs and pitchforks (PFs) occur.

5 Experimental Validation

Shown in Fig. 12 is the test bucket that was constructed to validate the predicted location and stability behavior of the vessel equilibrium positions. The bucket is attached to a pivot that allows rotation. The pivot can also be raised and lowered to vary the pivot height P.

The bucket is constructed of Lexan sheets. The top is left open to fill and empty the bucket. For structural integrity, all of the seams are reinforced with aluminum angle bars screwed into the corners. The seams are also sealed with silicone. On two sides of the bucket, two aluminum flat bars form tracks for the pivot. The pivot has two clamps that grasp the tracks and can be released to adjust the pivot height. The support structure has a wooden base and two aluminum angle bars cantilevered up to support the pivot point. At the pivot point, a ball-bearing ensures free rotation of the bucket. A good bearing is essential to get accurate and consistent results during the tests. In the theoretical derivations, the wall thickness was neglected. To minimize the influence of the mass of the bucket on the measurements, the center of gravity of the bucket was adjusted to coincide with the axis of the pivot. To achieve this, steel plates were attached to the bottom of the bucket.

The first step in running the tests was to set the pivot height to a specific value. Setting this parameter accurately is crucial for the results to be accurate because the equilibrium positions change significantly with small variations in the pivot height. The bucket was then filled with the desired amount of water. Next, the bucket was manually rotated to find the equilibrium points. The bucket settled on stable positions. Unstable positions were located by manually rotating the bucket until a point was found where the

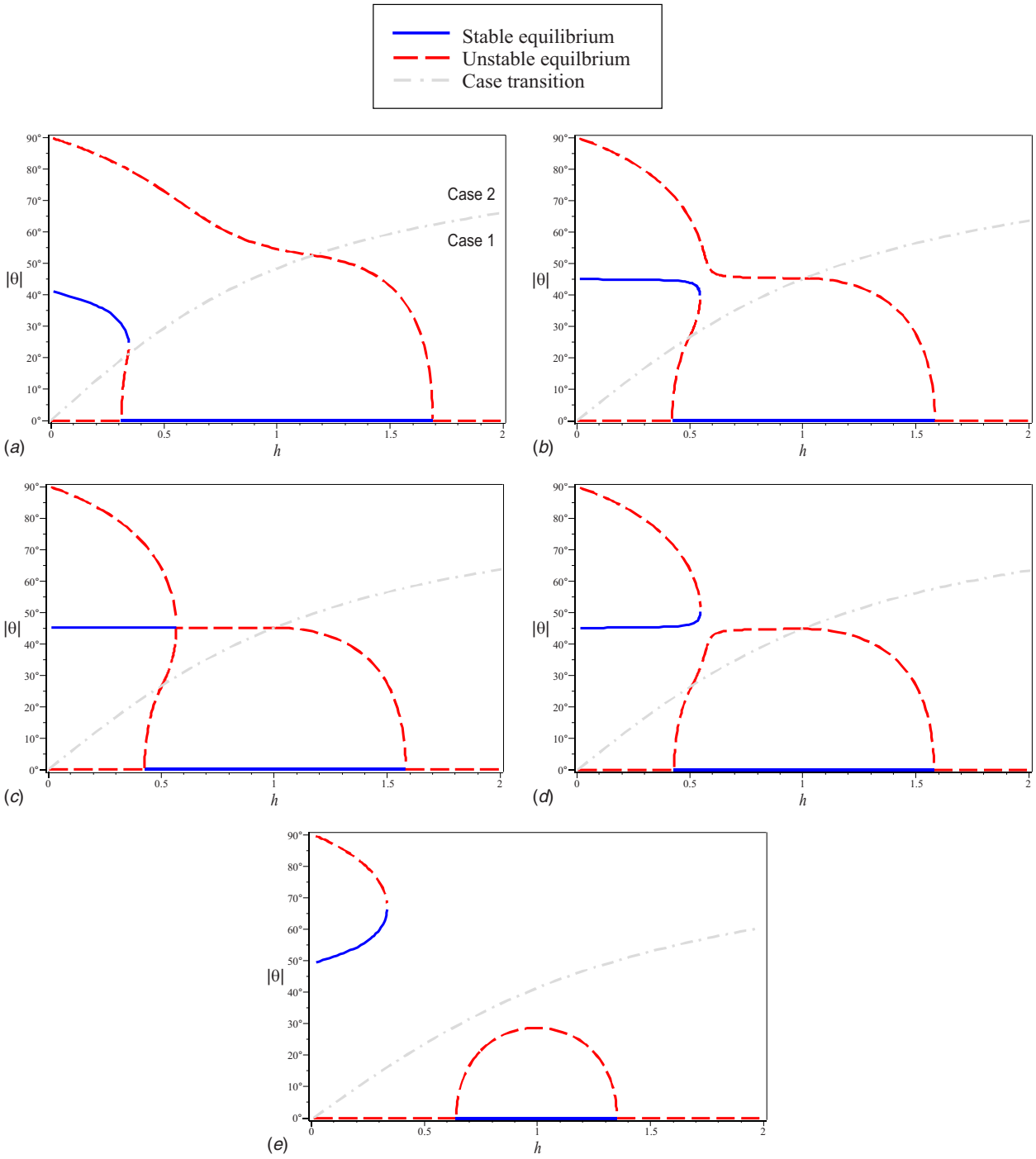

Fig. 10 Bifurcation diagrams

bucket tried to rotate in opposite directions on either side of a point. The angles were measured by a protractor attached to the support structure.

The angles were measured with an accuracy of ±1 deg. The water height (H), pivot height (P), and vessel width (W) were measured with precision of ±1.6 mm (±1/16 in.), ±1.6 mm (±1/16 in.), and ±0.8 mm (±1/32 in.), respectively. The precision of the nondimensional water height (h) evaluates to ±0.022, and the nondimensional vessel width (w) precision evaluates to ±0.032. The diagrams in Fig. 13 are the results of three tests run on the bucket. The points shown are the test results and the lines are the calculated predictions. The uncertainty in the measurements is not shown in the results.

The data from the experiments very closely follow the predicted trends. The areas, which were difficult to test, were where the pivot angle changes significantly with small changes in the water height, i.e., lines with steep slopes on the diagrams. This is evident in Fig. 13(a) where the unstable region near h=0.3 was not found and in Fig. 13(b) where only two unstable points were found near h=0.3. It should also be noted in Fig. 13(c) that there exists a region where no stable equilibria exist, which accounts for the liquid spilling immediately.

6 Dynamics With State Constraint

In this section, we are expanding our analysis from static stability to dynamic response. Understanding the unforced and

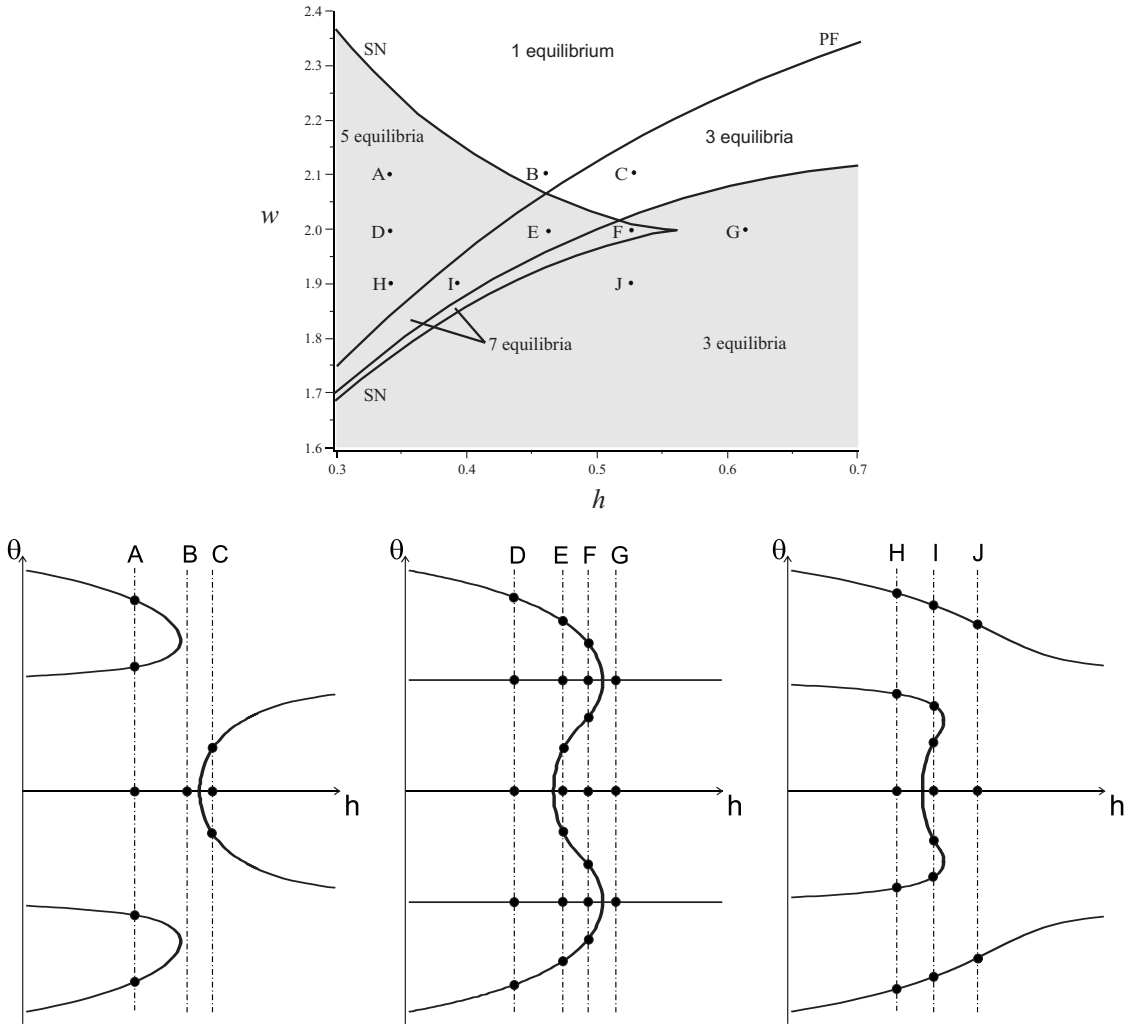

Fig. 11 Unfolding of the bifurcation diagrams near the cusp. Shaded region refers to case 2 equilibria existing.

forced behaviors of the system is important and yields insight into the design of vehicle fuel tanks or ballast tanks. The forcing that we consider is a vertical oscillatory acceleration of the vessel. This would be representative of a fuel tank in a vibrating vehicle such as a rocket undergoing pogo oscillation [10].

Since the cross section of the liquid volume changes as a function of the angle of rotation, the correct equation of motion would be one for deformable bodies [11]. Instead, here we develop the equation of motion based on Euler's equation for rigid bodies. The reason for this is that the aspect of the motion of the vessel we emphasize here is the state constraint on the angle; i.e., there is a threshold for the rotation at which the liquid will spill. Another simplifying assumption here is that there is no sloshing; i.e., the liquid volume will change its cross section in a quasistatic manner. Obviously, this is not a realistic assumption for even moderate velocities and accelerations.

With the above caveats, the equation of motion of the vessel is given by

$$I(\theta)\ddot{\theta} - (1 + A\cos(\omega t + \phi))(\boldsymbol{r}_{CG} \cdot \hat{i}) = 0 \tag{30}$$

Here $0 < A < 1$, ω, and ϕ are the amplitude,[2] frequency, and phase of the forcing, respectively. The nondimensional moment of inertia of the liquid cross section about the pivot point [12] is

$$I(\theta) = \frac{1}{6}\frac{\sum_{n=1}^{n=N-1} \|\vec{r}_{n+1} \times \vec{r}_n\|(\|\vec{r}_{n+1}\|^2 + \vec{r}_{n+1} \cdot \vec{r}_n + \|\vec{r}\|_n^2)}{\sum_{n=1}^{n=N-1} \|\vec{r}_{n+1} \times \vec{r}_n\|}. \tag{31}$$

Here N is the number of vertices ($N=4$ for the trapezoidal case and $N=3$ for the triangular case), and $\boldsymbol{r}$ are vectors from the pivot point to the vertices (refer to Sec. 2).

Let us define $p(\theta)$ as the ratio of the nondimensional moment arm and moment of inertia,

$$p(\theta) \equiv -\frac{\boldsymbol{r}_{\mathrm{CG}} \cdot \hat{i}}{I(\theta)} \tag{32}$$

Although $p(\theta)$ is a complicated transcendental function (see Fig. 14), the essential features (local minimum, maximum, and zero) of this ratio can be well captured by polynomial approximations, denoted by $\bar{p}(\theta)$.

Using the polynomial approximation, the equation of motion becomes

$$\ddot{\theta} + (1 + A\cos(\omega t + \phi))\bar{p}(\theta) = 0 \tag{33}$$

subject to

[2] $A > 1$ would result in the liquid losing contact with the vessel.

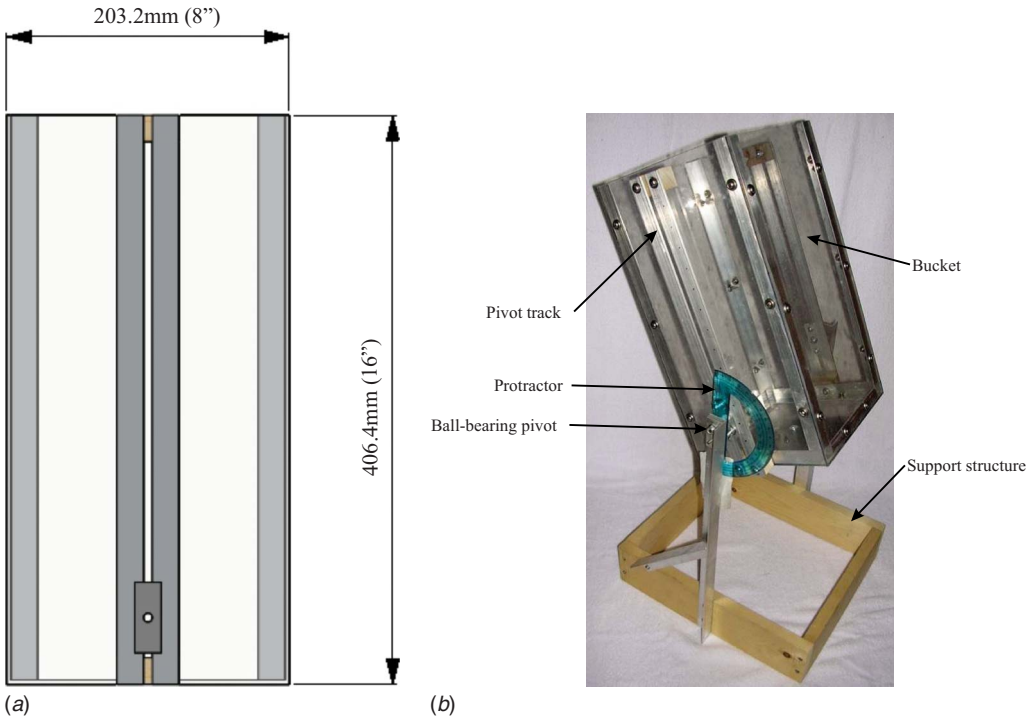

Fig. 12 Test bucket design and apparatus

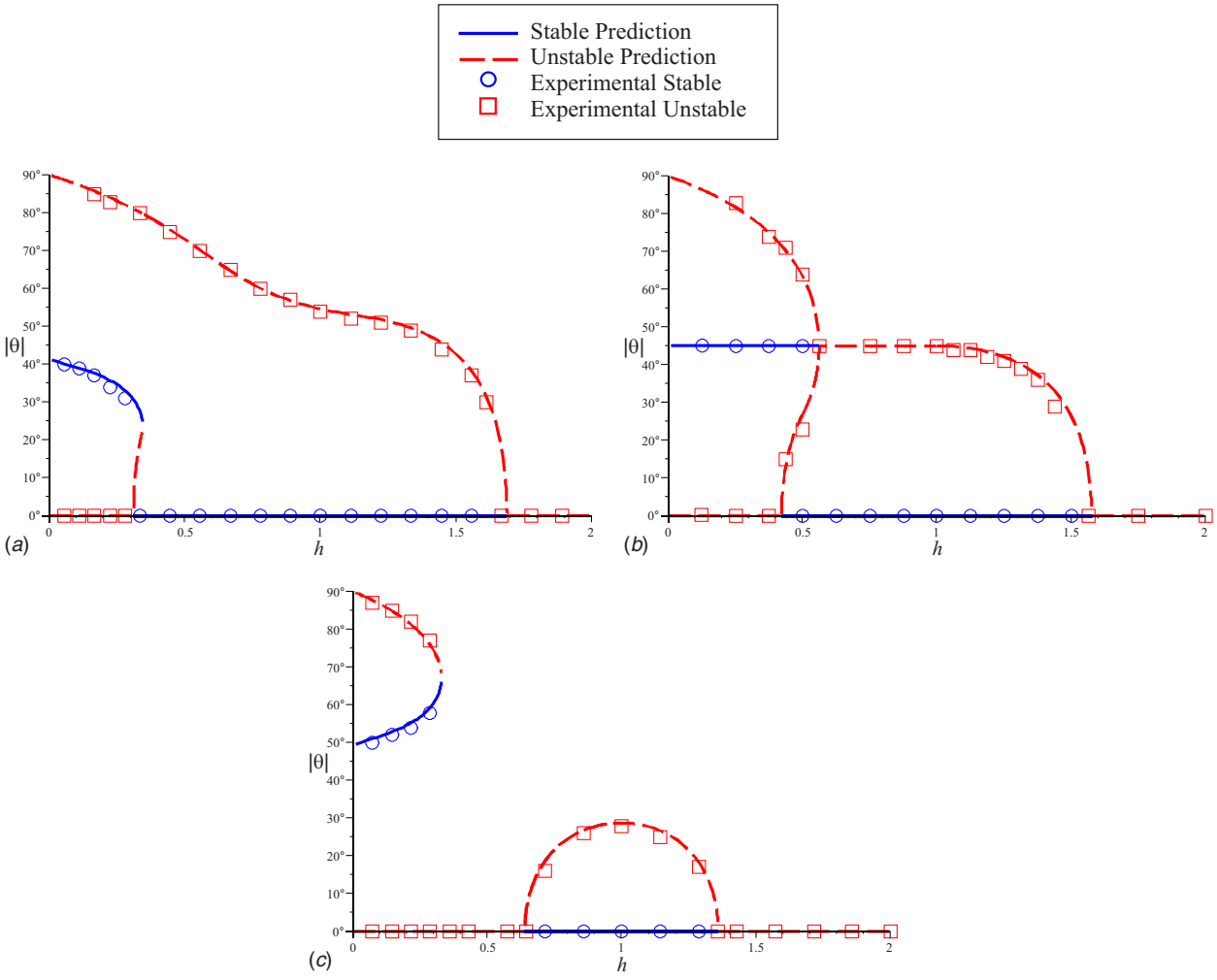

Fig. 13 Experimental results

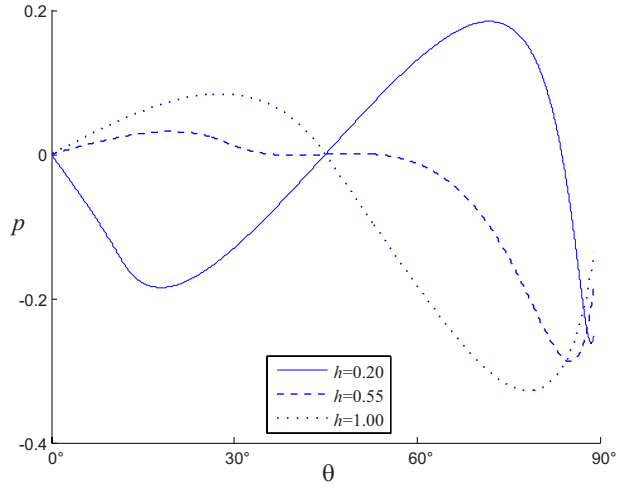

Fig. 14 Plots of $p(\theta)$ for $w=2$ and various h values

$$|\theta| \leq \theta_t \tag{34}$$

This parametrically forced differential equation is in the form of a nonlinear Mathieu-type equation with a state constraint. The constraint (34) codifies the limitation that the liquid will spill as the angle reaches the *spill threshold* θ_t.

7 Unforced and Forced Response

The unforced system, Eq. (33) with $A=0$, is given by

$$\ddot{\theta} + \bar{p}(\theta) = 0 \tag{35}$$

This is a conservative system (no friction at the pivot point, nor damping from sloshing). The total energy E can be expressed as

$$E = \frac{1}{2}\dot{\theta}^2 + \int \bar{p}(\theta) d\theta \tag{36}$$

The phase plot in Fig. 15(a) resembles that of the well-known pendulum equations. While the pendulum trajectories can be classified as librations, heteroclinic trajectories, and rotations, for the vessel we observe librations, heteroclinic paths, and trajectories bounded in time. No rotations are possible, since those trajectories would reach the spill threshold. This marks the fundamental difference between the vessel and a pendulum. As shown in Figs. 15(b) and 15(c), when more than three equilibria exist, the phase plot deviates from the typical pendulum phase portrait, for example, in Fig. 15(b), the origin is a saddle instead of a center [13–15].

Now we examine the effect of forcing on the dynamics of the vessel. Figure 16 shows projected trajectories in the $t-\theta$ and $\theta-\dot{\theta}$ planes. One can observe many trajectories that terminate at the spill threshold.

To characterize time-bounded trajectories, we introduce the notion of life expectancy of trajectories, which we define as the time it takes for a trajectory to reach the spill threshold. Librations and heteroclinic orbits never reach the spill threshold; therefore, the life expectancy of these trajectories is infinite. Life expectancy plots in Fig. 17 show lifespans of trajectories for given initial conditions in the $\theta-\dot{\theta}$ plane. Due to the computational expense of creating these plots, integration was carried out for 30 time units.

As a general observation, near the centers of the unforced system libration trajectories, shown in Fig. 15, the vessel is less likely to spill, whereas away from the unforced libration trajectories, the vessel spills quickly. These lifespan plots also show some irregular trends, notably very small paths where spilling does not occur over many time units. For clarity, we zoom in on these points in Fig. 18.

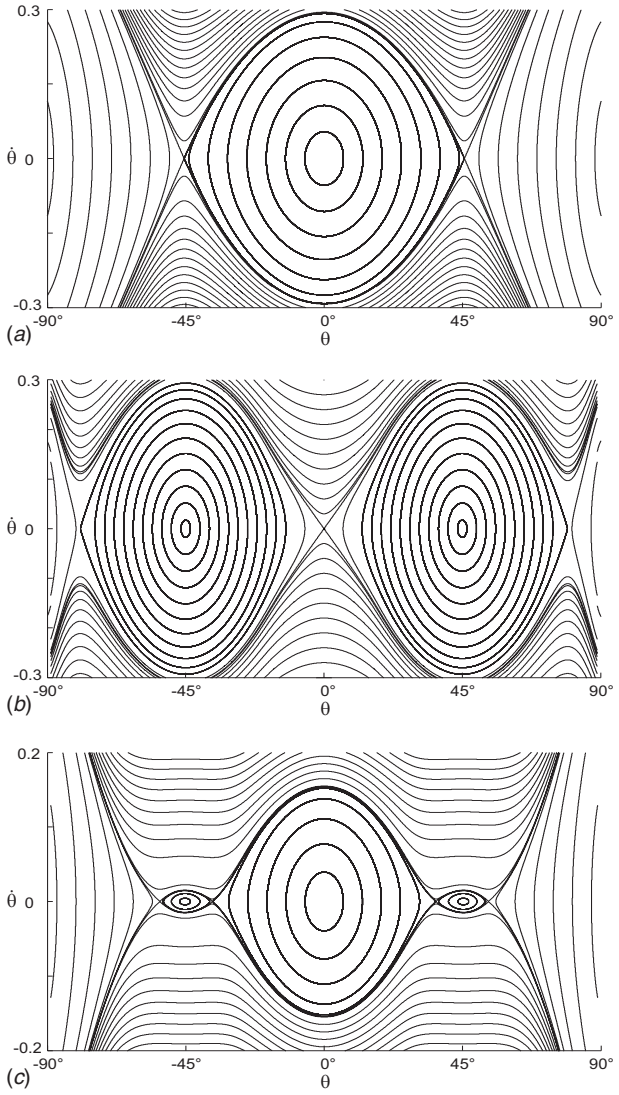

Fig. 15 Unforced phase plot of the equation of motion for $w=2.0$

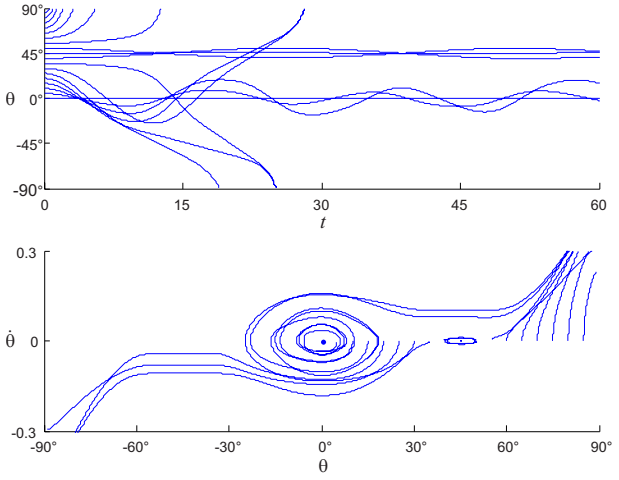

Fig. 16 Example trajectories for $h=0.55$, $w=2$, $\omega=0.5$, $A=0.5$, $\phi=0$

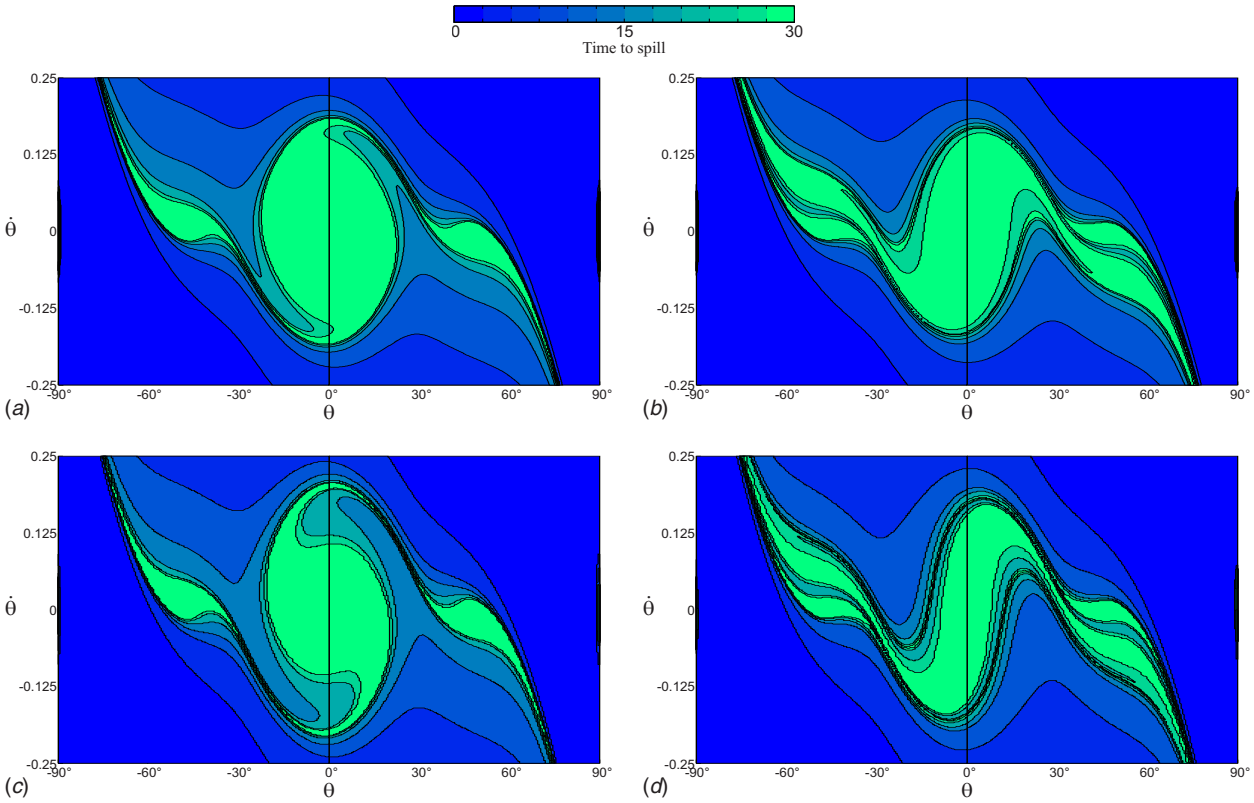

Fig. 17 Lifespan of trajectories for various initial conditions, amplitudes, and frequencies for h=0.55 and w=2. The color scale denotes the lifespan in time units.

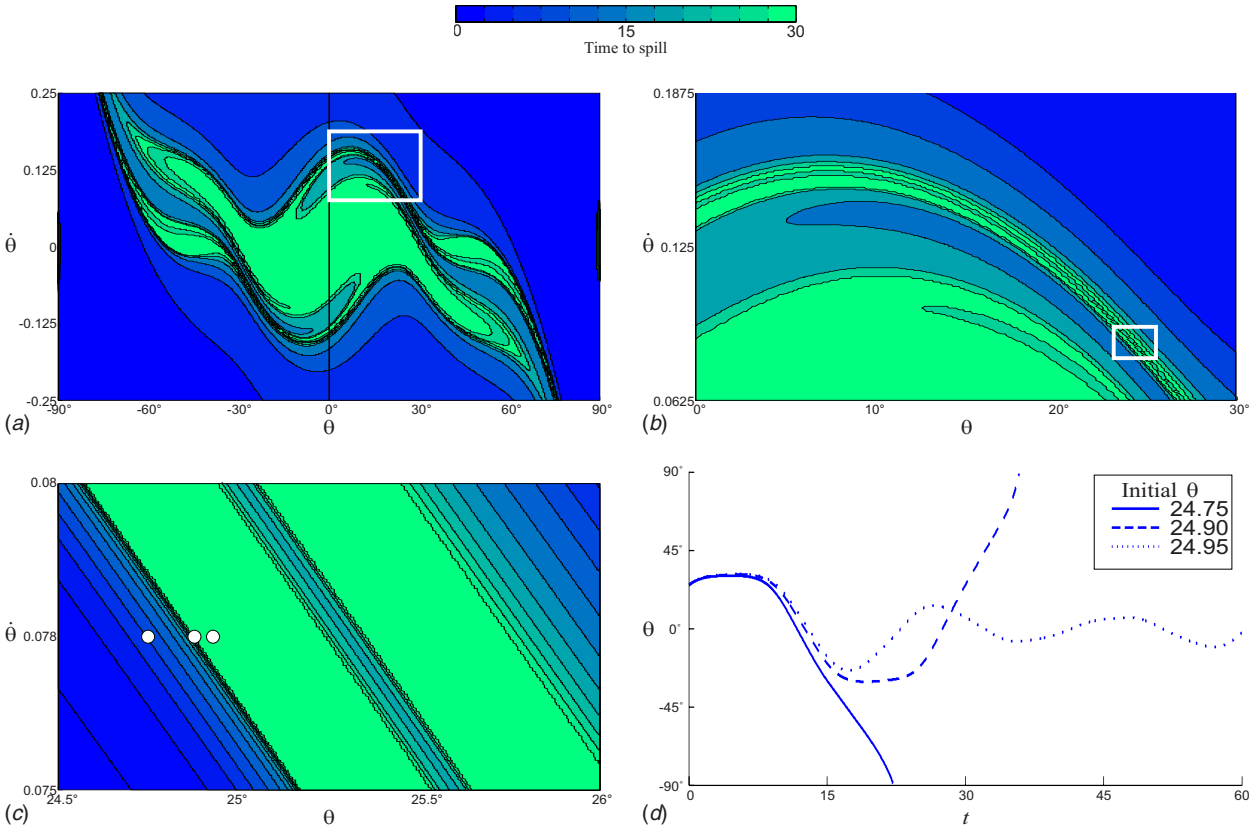

Fig. 18 Zooming in on the lifespan plot for ω=0.75, A=0.75, ϕ=0. The three initial conditions for (d) are marked on (c).

8 Concluding Remarks

The vessel-liquid system analyzed in this paper has been shown to have co-existing (up to seven) equilibria under many conditions. Closed-form conditions for the existence of various numbers of equilibria were given and the corresponding domains in the h-w plane were illustrated. A simple stability condition for $\theta = 0$ was also found, which provided information about the stability of all co-existing equilibria. The existence of subcritical pitchfork and saddle-node bifurcations was proven and bifurcation diagrams were constructed, together with a detailed unfolding of the bifurcation diagrams around the cusp point. To experimentally validate the findings, a rectangular cross section bucket mounted on a pivot was used. Experimental data agree very well with the theoretically predicted equilibrium positions and their stability.

A simplified equation of motion, a Mathieu equation with a state constraint, was derived. The response of the system was presented in the $\theta - \dot{\theta}$ and $t - \theta$ plots. These plots showed trajectories that terminate at the state constraint. This invoked the notion of lifespan. Plots were shown that express the lifespan as a function of the initial conditions of the vessel. The lifespan was shown to change drastically for small changes in initial conditions. A detailed analysis of the deformable body dynamics and further discussion of the state constraint and lifespan will be the topic of a forthcoming paper.

Acknowledgment

Valuable discussions on the topic with Gábor Stépán and financial support by the U.S. Air Force Office of Scientific Research (Grant No. AFOSR-06-0787) are gratefully acknowledged. We also thank the reviewers for their insightful comments.

References

[1] Warmowska, M., 2006, "Numerical Simulation of Liquid Motion in a Partly Filled Tank," Opuscula Mathematica, **26**(3), pp. 529–540.
[2] Stépán, G., and Bianchi, G., 1994, "Stability of Hanging Blocks," Mech. Mach. Theory, **29**(6), pp. 813–817.
[3] Duffy, B., 1993, "A Bifurcation Problem in Hydrostatics," Am. J. Phys., **61**(3), pp. 264–269.
[4] Erdös, P., Schibler, G., and Herndon, R., 1992, "Floating Equilibrium of Symmetrical Bodies and Breaking of Symmetry," Am. J. Phys., **60**(4), pp. 335–356.
[5] Delbourgo, R., 1987, "The Floating Plank," Am. J. Phys., **55**(9), pp. 799–802.
[6] Hale, J., and Koçak, H., 1991, *Dynamics and Bifurcations*, 3rd ed., Springer-Verlag, Berlin.
[7] Rorres, C., 2004, "Completing Book II of Archimedes' On Floating Bodies," Math. Intell., **26**(3), pp. 32–42.
[8] Strogatz, S. H., 2001, *Nonlinear Dynamics and Chaos*, 1st ed., Westview Press, Boulder, CO.
[9] Guckenheimer, J., and Holmes, P., 1990, *Nonlinear Oscillations, Dynamical Systems, and Bifurcations of Vector Fields*, 3rd ed., Springer, New York.
[10] Oppenheim, B. W., and Rubin, S., 1993, "Advanced Pogo Stability Analysis for Liquid Rockets," J. Spacecr. Rockets, **30**(3), pp. 360–373.
[11] McDonough, T. B., 1976, "Formulation of the Global Equations of Motion," AIAA J., **14**, pp. 656–660.
[12] Bockman, S. F., 1989, "Generalizing the Formula for Areas of Polygons to Moments," Am. Math. Monthly, **96**(2), pp. 131–132.
[13] Gilbert, E. N., 1991, "How Things Float," Am. Math. Monthly, **98**(3), pp. 201–216.
[14] Moseley, H., 1850, "On the Dynamical Stability and on the Oscillations of Floating Bodies," Philos. Trans. R. Soc. London, **104**, pp. 609–643.
[15] Poston, T., and Stewart, J., 1996, *Catastrophe Theory and Its Applications*, Dover, Berlin.